Crystal structures and sodium/silver distributions within the ionic conductors $Na_5Ag_2Fe_3(As_2O_7)_4$ and $Na_2Ag_5Fe_3(P_2O_7)_4$†

Eric Quarez,*[a] Olivier Mentré,[b] Karim Djellab[a] and Christian Masquelier[a]

Received (in Montpellier, France) 21st July 2009, Accepted 3rd September 2009
First published as an Advance Article on the web 24th November 2009
DOI: 10.1039/b9nj00355j

The crystal structures of new $Na_5Ag_2Fe_3(As_2O_7)_4$ and $Na_2Ag_5Fe_3(P_2O_7)_4$ compounds, prepared through ion exchange from $Na_7Fe_3(X_2O_7)_4$ (X = P, As) are reported. They crystallize in the monoclinic $C2/c$ space group and exhibit a Na/Ag ordering on cooling. Crystal structures were determined from single crystal X-ray diffraction at 100 and 298 K for each composition. The structure consists of FeO_6 octahedra sharing their corners with X_2O_7 dimers (X = P, As) to form a three-dimensional framework $[Fe_3(X_2O_7)_4]^{7-}$ into which the sodium/silver ions are located. The differences between the four structures lie on the distribution of the sodium/silver ions within this framework giving a developed insight of the ionic diffusion paths.

Introduction

Phosphate compositions and structures have been widely investigated recently for their high silver ionic conduction. These include open structures of "NASICON"-type such as $Ag_{1+x}Zr_{2-x}M_x(PO_4)_3$ M = Sc, Fe,[1] $AgTaMP_3O_{12}$[2] (M = Al, Ga, In, Cr, Fe and Y), $AgSbMP_3O_{12}$ (M = Al, Ga, Fe and Cr)[3] and of other structural families such as $(Ag_{1-x}Na_x)_2FeMn_2(PO_4)_3$,[4] $Ag_2VP_2O_8$[5] and $AgRu_2(P_2O_7)_2$.[6] The high ionic conductivity of these ceramics can be used in devices such as membranes, fuel cells and gas sensors.[7–9] The other potential applications include low thermal expansion behavior,[10] hosts for radioactive waste,[11] catalyst supports,[12] ion exchangers[13,14] and insertion/extraction reactions.[15–17]

Recently, we reported the crystal structure of two new silver ion conductors, $Ag_7Fe_3(X_2O_7)_4$ (X = P, As),[18] parents of the sodium analogs published several years ago.[19–21] $Ag_7Fe_3(X_2O_7)_4$ crystals were obtained by complete Na^+/Ag^+ exchange reactions between $Na_7Fe_3(X_2O_7)_4$ and molten $AgNO_3$ at 600 K. Both $Ag_7Fe_3(X_2O_7)_4$ (X = P, As) compositions undergo a reversible $\alpha \leftrightarrow \beta$ phase transition associated with a loss of silver ion ordering upon heating, associated with an increase of the crystal symmetry, from primitive P to C-centered lattice.[18] Refinements of thermal displacement parameters reveal the strong anisotropy of Ag^+ motion (mostly bi-dimensional) with favored diffusion paths, based on bond valence sum (BVS) calculations. As proposed earlier,[19–21] the $[Fe_3(X_2O_7)_4]_\infty$ framework is indeed built on "A" and "B" layered subunits parallel to (001), delimiting π conduction planes (Fig. 1). Proposed silver diffusion paths indicate easy motion inside and between neighboring π planes of the A layers. On the other hand, diffusion across the "B" layer parallel to [001]* appears rather unlikely.

This family of phosphate and arsenate "bidimensional" frameworks exhibits a very high affinity towards silver cations which allows a monitoring of the $Ag^+ \Leftrightarrow Na^+$ cation exchange ratio through the respective amounts of Na^+ in the solid and Ag^+ in aqueous solution of $AgNO_3$. In other words, the number, x, of Ag^+ cations that can be incorporated in the structure according to $Na_{7-x}Ag_xFe_3(X_2O_7)_4$ is governed by the amount of Ag^+ in the $AgNO_3$ solution into which the powder is immersed. This compositional monitoring is of course reminiscent of strong cationic mobility in the framework; the basis of our prior and present investigations.[18–21]

The seven sodium atoms in $Na_7Fe_3(X_2O_7)_4$ are distributed on various crystallographic sites, as follows: five sodium ions are located within the A layers into mostly partially occupied sites; two sodium ions are located within the B layers, into the fully-occupied Na(1) site (Fig. 1). Within the whole series of

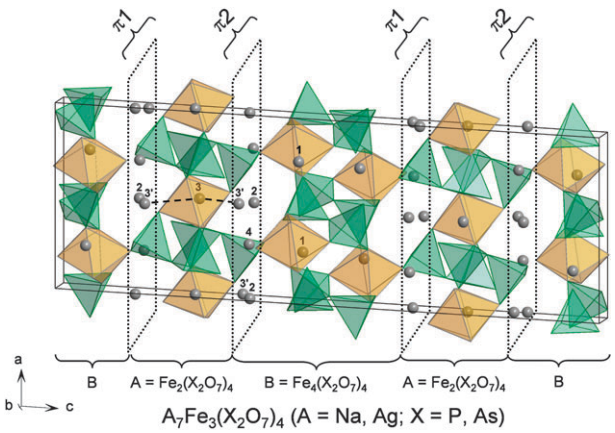

Fig. 1 Projection along [010] of the idealized structure of $A_7Fe_3(X_2O_7)_4$ (A = Ag, Na; X = P, As). The A sites are numbered. The picture indicates the location of the A and B layers and the π planes at $z \sim 0.15$ and 0.35.

[a] *Laboratoire de Réactivité et Chimie des Solides, CNRS UMR 6007, Université de Picardie Jules Verne, 33 rue St. Leu, 80039 Amiens cedex, France. E-mail: Eric.Quarez@cnrs-imn.fr*
[b] *UCCS, Equipe Chimie du Solide, CNRS UMR 8181, ENSC Lille—UST Lille, BP 90108, 59652 Villeneuve d'Ascq cedex, France*

† Electronic supplementary information (ESI) available: Tables of atomic parameters, displacement parameters and selected inter-atomic distances for $Na_5Ag_2Fe_3(As_2O_7)_4$ and $Na_2Ag_5Fe_3(P_2O_7)_4$ at 100 K and 298 K. CCDC reference numbers 748060–748063. For ESI and crystallographic data in CIF or other electronic format see DOI: 10.1039/b9nj00355j

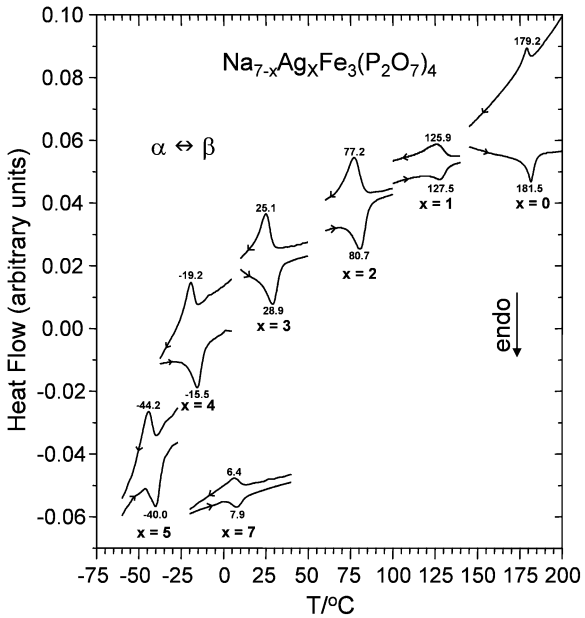

Fig. 2 DSC plots of $Na_{7-x}Ag_xFe_3(P_2O_7)_4$ ($0 \leq x \leq 7$, except for $x = 6$) exhibiting reversible phase transition temperatures.

compositions, $Na_{7-x}Ag_xFe_3(P_2O_7)_4$ ($x = 0$ to 7), the temperature at which the α ⇔ β transition occurs depends strongly on x, as demonstrated in Fig. 2. It decreases in a regular manner as x increases from 0 to 5, as a result of the substitution of Na^+ by Ag^+ which shows intrinsically better diffusion properties into this kind of framework. Hence, at 298 K, sodium-rich $Na_{7-x}Ag_xFe_3(P_2O_7)_4$ compositions show a long-range ordering of Na^+/Ag^+ cations at room temperature (α form) while silver-rich ones are disordered (β form).

In this paper, we focus on the single crystal structure study, at various temperatures, of two members of the $Na_{7-x}Ag_xFe_3(X_2O_7)_4$ family, *i.e.* $Na_5Ag_2Fe_3(As_2O_7)_4$ and $Na_2Ag_5Fe_3(P_2O_7)_4$ in order to get a deeper insight on the mechanism of ionic conduction of these compounds *via* a precise analysis of preferential ion exchange reactions (favored crystallographic sites) and anisotropic thermal motion within the possible conduction paths.

Experimental

Single crystals of the parent compositions, $Na_7Fe_3(X_2O_7)_4$ (X = P, As), were preliminary grown by slow cooling (~2° h^{-1}) from ~750 to 500 °C and then faster down to room temperature, within a flux of sodium phosphates or arsenates in excess, as indicated in detail in ref. 19 and 20. Single crystals of $Na_{7-x}Ag_xFe_3(P_2O_7)_4$ ($0 < x \leq 7$) and $Na_5Ag_2Fe_3(As_2O_7)_4$ were then prepared by ion exchange using $AgNO_3$ solutions with appropriate concentrations and volumes, followed by potentiometry: the remaining Ag^+ concentration was tracked by an Ag/Hg_2SO_4 blended electrode. In less than ~1/2 h of stirring, the number of moles of silver remaining in solution was close to ~0 with a Na^+/Ag^+ exchange percentages varying from 97 to 99%, depending on the value of x. The nitrate solution was then eliminated and another rinsing with H_2O was performed. Finally, the single crystals were dried in an oven. Some of the exchanged crystals were selected for structural studies, some were ground to fine powders so as to perform differential scanning calorimetry (DSC) and powder X-ray diffraction (XRD) experiments.

DSC measurements were carried out on ~20 mg of powder using a NETZSCH DSC 204 F1 analyzer at temperatures varying from 173 to 773 K with heating and cooling rates of 10 °C min^{-1}. For phosphates, almost all compounds undergo a reversible phase transition in the temperature range −50 to 185 °C (Fig. 2 and Table 1). From $x = 0$ to 5, the transition temperature goes down gradually from 178 to −46 °C. For $x = 7$, the transition temperature goes above 0 °C at 2.9 °C. For $x = 6$ phosphate and $x = 2$ arsenate, DSC measurements did not reveal any significant thermal effect in the temperature range. As for $Ag_7Fe_3(As_2O_7)_4$,[18] this suggests that the β → α transition takes place below −100 °C.

Powder XRD patterns were collected at 298 K on a θ–θ Bruker D8 diffractometer using the Co Kα1,2 radiation (Göbel mirror, radial slits and PSD counter) between 2θ = 10 and 60° at 8 s per step of 0.02°. Temperature-controlled X-ray diffraction under flowing N_2 was also performed using an Anton Parr Chamber HTK 1200 °C. X-ray diffraction patterns were recorded at 40 and 90 °C. Between each fixed temperature, the powder was heated at a rate of 6 °C min^{-1}. The same conditions were used on cooling and a diffraction pattern was recorded at 50 °C.

The XRD patterns of $Na_{7-x}Ag_xFe_3(P_2O_7)_4$ ($0 < x < 7$) recorded at 298 K were analyzed by using the pattern matching mode of the Fullprof suite.[22] All members adopt the monoclinic space group $C2/c$ with refined lattice parameters and volumes indicated in Table 1. Compositions with $0 \leq x \leq 2$ are isostructural with the α form of $Na_7Fe_3(P_2O_7)_4$, *i.e.* indexed in a supercell (~6600 $Å^3$) due to long range ordering of "mobile" cations. At room temperature, for $3 \leq x \leq 7$, the β-form is adopted at 298 K. This is clearly illustrated in Fig. 3 which, in particular, shows the very high number of diffraction peaks of $Na_5Ag_2Fe_3(P_2O_7)_4$ that cannot be indexed in the "average" β-form unit cell. As proposed in ref. 19–21, the structural relationships between the α form ($\vec{a}$, $\vec{b}$, $\vec{c}$) and the β form ($\vec{a}_0$, $\vec{b}_0$, $\vec{c}_0$) are given by: $\vec{a} = 3\,\vec{a}_0$, $\vec{b} = \vec{b}_0$; and $\vec{c} = -\vec{a}_0 + \vec{c}_0$. Interestingly, the intensities of the diffraction lines characterizing the superstructure grow progressively from $x = 0$ to 2, *i.e.* as the amount of Ag^+ increases (dominant *vs.* Na^+ for scattering factors). Fig. 4 shows the nice reversibility of the α ↔ β transition through XRD patterns recorded successively at 40, 90 and 50 °C. This is in full agreement with the transition temperature (77 °C) determined by DSC (Fig. 2). For the members $x = 3$ to 6, the patterns were indexed in the disordered form of β-$Ag_7Fe_3(P_2O_7)_4$ ($x = 7$).

Single crystal analysis: energy-dispersive spectroscopy (EDS) analysis performed on the single crystals selected for the structural studies were consistent with the formula of $Na_5Ag_2Fe_3(As_2O_7)_4$ and $Na_2Ag_5Fe_3(P_2O_7)_4$. The diffraction intensities were collected at low temperature (~100 K) using a Bruker SMART CCD 1 K diffractometer, Mo Kα radiation, equipped with an OXFORD cryostream 700 for data collection. At 298 K, a Bruker X8 diffractometer was used.

Table 1 Phase transition temperature $T\varphi$, cell parameters, volume and number of formula units in unit cell (Z) in $C2/c$ space group at 298 K (powder data) for $Na_{7-x}Ag_xFe_3(P_2O_7)_4$ ($0 \leq x \leq 7$) compounds

x	0	1	2	3	4	5	6	7
$T\varphi$/°C	178.5	122.7	75.0	23.2	−21.6	−46.0	—	2.9
Ref.	20	This work	This work	This work	This work	This work	This work	18
a/Å	28.519(3)	28.537(4)	28.5485(1)	9.527(2)	9.530(2)	9.535(2)	9.547(3)	9.5561(5)
b/Å	8.333(2)	8.353(1)	8.3585(1)	8.364(1)	8.370(1)	8.387(1)	8.398(3)	8.4417(4)
c/Å	29.834(5)	29.912(4)	29.9870(3)	27.944(4)	28.014(5)	28.099(3)	28.182(9)	28.226(1)
β/°	111.88(1)	111.95(1)	112.028(1)	93.65(1)	93.66(1)	93.64(1)	93.64(1)	93.465(2)
V/Å^3/Z	6579(4)/12	6613.4(2)/12	6633.2(3)/12	2222(1)/4	2229(1)/4	2242(1)/4	2255(2)/4	2272.8(3)/4
Volume average structure/Å^3	2193(1)	2204(1)	2211(1)					

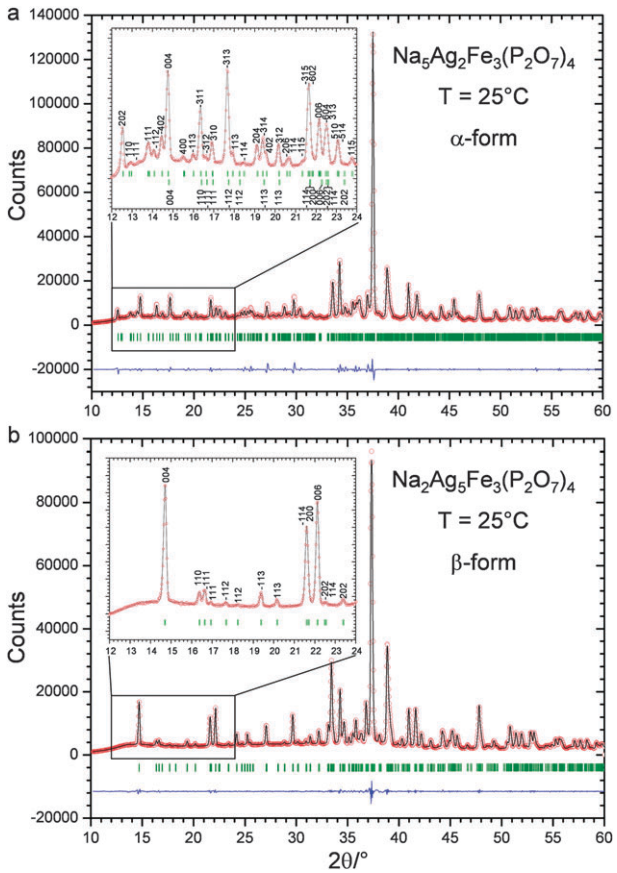

Fig. 3 Observed (red markers) and calculated (black solid line) powder X-ray diffraction patterns and their difference (blue line) at 298 K for α-$Na_5Ag_2Fe_3(P_2O_7)_4$ (a) and β-$Na_2Ag_5Fe_3(P_2O_7)_4$ (b) *hkl* indexes are given for the observed lines. In the inset of graph a, the indexes of the average structure unit cell are indicated highlighting the superstructure lines.

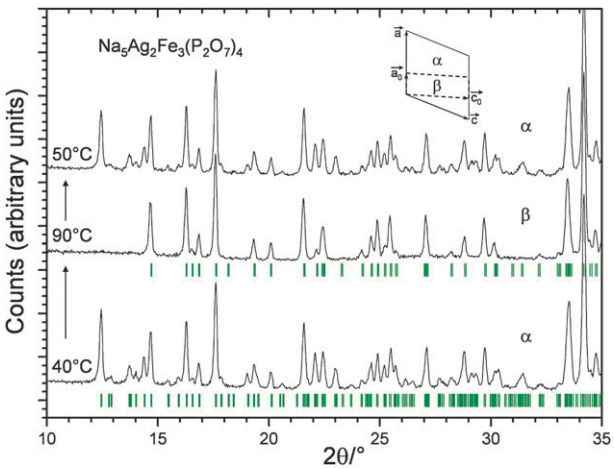

Fig. 4 Powder XRD patterns for $Na_5Ag_2Fe_3(P_2O_7)_4$ on temperature cycling. The reversible α → β phase transition is exhibited by the disappearance of the supercell lines on heating at 90 °C and their subsequent reappearance on cooling at 50 °C. The green markers indicate the Bragg positions of the α and β forms. The geometric relationship between the average structure unit cell (a_0, b_0, c_0) and the superstructure unit cell (a, b, c) is shown. The refined cell parameters in the space group $C2/c$ for the data collected at 40, 90 and 50 °C are, respectively: a = 28.5494(2) Å, b = 8.3598(1) Å, c = 29.995(1) Å, β = 112.072(3)°; a = 9.517(1) Å, b = 8.3609(3) Å, c = 27.865(2) Å, β = 93.645(1)° and a = 28.5501(2) Å, b = 8.3600(1) Å, c = 29.9981(1) Å, β = 112.075(2)°.

The global experimental parameters for the four crystal structures determined are gathered in Table 2. The SMART software[23] was used for the data acquisition and SAINT[24] for data extraction and reduction. An absorption correction based on face indexation was then applied using the program Xprep of the SHELXTL package.[25] An additional correction for absorption based on symmetry equivalent reflections was subsequently applied with the program SADABS.[26] The crystal structure solution and refinement processes were carried out with SHELXS[25] and JANA2006,[27] respectively.

Four data sets were recorded from two single crystals of $Na_5Ag_2Fe_3(As_2O_7)_4$ and $Na_2Ag_5Fe_3(P_2O_7)_4$, at 100 and 298 K.

(A) Crystal structure refinements

The refinements at room temperature were done by considering a split distribution of Ag/Na sites (*vs.* an anharmonic model) for the same reasons as those explained in detail in ref. 18: comparable R values for a lower number of refined parameters, no correlation between parameters and stable refinement with easy convergence for the split model. For example: $Na_2Ag_5Fe_3(P_2O_7)_4$—split (Ag3′-Ag3″-Ag3‴, Ag4-Ag4′-Ag4″): R = 2.62%, $n_{param.}$ = 255 —harmonic: (Ag3: 4th order, Ag4: 4th order) R = 2.64%, $n_{param.}$ = 269.

(A1) $Na_5Ag_2Fe_3(As_2O_7)_4$ (x = 2): analysis of the β′ → β transition. At 298 K, the crystal structure of $Na_5Ag_2Fe_3(As_2O_7)_4$ (β form) has been successfully refined

Table 2 Crystal data, data collection and structure refinement parameters for $Ag_2Na_5Fe_3(As_2O_7)_4$ and $Ag_5Na_2Fe_3(P_2O_7)_4$ at 100 and 298 K

	$Ag_2Na_5Fe_3(As_2O_7)_4$ (x = 2)		$Ag_5Na_2Fe_3(P_2O_7)_4$ (x = 5)	
T/K	100	298	100	298
M_r/g mol^{-1}	1545.58	1545.58	1448.63	1448.63
Crystal symmetry	Monoclinic	Monoclinic	Monoclinic	Monoclinic
Space group	$C2/c$ (n° 15)	$C2/c$ (n° 15)	$C2/c$ (n° 15)	$C2/c$ (n° 15)
a/Å	9.973(2)	9.9512(3)	28.551(5)	9.5375(3)
b/Å	8.549(2)	8.5741(2)	8.363(1)	8.3886(3)
c/Å	28.664(6)	28.8231(8)	30.064(6)	28.0971(9)
β/°	94.152(3)	93.910(1)	111.890(3)	93.623(2)
V/Å^3	2437.6(8)	2453.5(1)	6661(2)	2243.4(3)
Z	4	4	12	4
Number of measured reflections	9766	54142	21371	54056
Number of independent reflections [$I > 3\sigma(I)$]	2522	7600	2803	4784
R merging factor (%)	3.58	3.40	7.10	3.32
R_1 (F) [$I > 3\sigma$(I)] (%)[a]	2.64	3.11	5.45	2.62
wR_2 (F^2) [$I > 3\sigma(I)$] (%)[b]	2.73	3.20	5.66	2.64

[a] $R_1(F) = \sum||F_o| - |F_c||/\sum|F_o|$. [b] $wR_2(F^2) = [\sum w(F_o^2 - F_c^2)^2/\sum w(F_o^2)]^{1/2}$.

in the $C2/c$ space group in the same unit cell as for β-$Na_7Fe_3(As_2O_7)_4$.[19] Interestingly, the substitution of Na^+ by Ag^+ occurs (at this level of substitution) only within the Na2 and Na4 sites, *i.e.* within the crystallographic sites which are located on the π diffusion planes. Sodium in the Na1 site, previously expected[18–21] to be the least mobile of the structure, stays more or less as a spectator of the ionic exchange, as its occupancy remains 1 and no silver appears to be located in that site. Interestingly, Fourier maps reveal a strong splitting of the Na3′ and M4 sites into Na3′–Na3″ and M4/M4′ positions. Equivalent isotropic displacement parameters, BVS and selected interatomic distances for sodium/silver atoms are reported in Table 3.

At 100 K, the crystal structure of $Na_5Ag_2Fe_3(As_2O_7)_4$ has also been successfully refined in the $C2/c$ space group, in the same unit-cell as for β-$Na_5Ag_2Fe_3(As_2O_7)_4$. The absence of any supercell tripling down to 100 K corroborates the DSC measurements which reveal no significant thermal effect for this composition in the investigated thermal domain. Consequently, the initial atomic coordinates of Fe, As and O were taken as those of the "standard" β-phases. The heaviest electron density peaks calculated by Fourier difference allowed the silver ions to be located. Their occupancies were refined and found to be located on Na2/Ag2 and Na4/Ag4 mixed sites. Subsequent Fourier difference calculations allowed to locate the sodium ions on the Na1 (8g) site in the B layer and on the Na3 (4e) site in the A layer between two π planes. Both sodium occupancies on Na1 and Na3 sites were set at 1 before refinement which led to values of 0.99 and 0.98 respectively, hence fixed at 1 in the end. As the formula is sodium-deficient, restriction of the Na/Ag composition was considered according to the $Na_5Ag_2Fe_3(As_2O_7)_4$ formula. It is noteworthy that, compared with the structure of the β form determined at 298 K, the so-called M3′ and M3″ sites at the apex of Na3 in π-planes are empty at 100 K, as well as the M4′ site. Therefore, although no new superstructure reflections were found at 100 K, we can propose labelling $(Na_5Ag_2Fe_3(As_2O_7)_4)_{100\ K}$ as β′, characterized by an ordered distribution of vacancies on the M(3′–3″) site. In the last cycles of refinement, anisotropic atomic displacement parameters were applied to all atoms while isotropic secondary extinction was considered. The crystal, collection and refinement data are listed in Table 2. Equivalent isotropic displacement parameters and BVS for Ag^+ and Na^+ calculated from Brown and Altermatt data[28] are tabulated in Table 4. The distribution of the cationic sites in the π-planes is shown on Fig. 5 with probable diffusion paths contouring the AsO_4 groups. At this point, one should distinguish between crossroad-like M4 positions and midpath-like M2 and M3′ positions.

A brief summary of the cationic distribution arising from the β′ → β transition can be announced from these results but will be more detailed in the discussion. The Ag for Na substitution first concerns both midpath-like M2 and crossroad-like M4 while M3′/M3″ remains empty, these latter being at the apex of fully-occupied Na3 particular sites. On heating, Na3′/Na3″ is progressively occupied from the Na3 → Na3′ and Na4 → Na3′ diffusions. This is accompanied by the site splitting of M4 into M4 and M4′ positions. At 298 K, the relative occupancy of each site suggests a preferential location of sodium in midpath sites while the 2 silver content

Table 3 Wyckoff positions, site occupation factors (SOF), bond valence sums, equivalent isotropic displacement parameters and selected interatomic distances for sodium/silver atoms in β-$Ag_2Na_5Fe_3(As_2O_7)_4$ (x = 2) at 298 K. * refined close to unity

Atom	Wyck.	SOF	BVS	U_{eq}[a]/Å^2
Na1	8f	1*	1.082(3)	0.0150(3)
Ag2/Na2	8f	0.35(1)/0.65	0.943(2)/0.849(2)	0.0266(2)
Na3	4e	0.48(1)	1.127(4)	0.035(2)
Na3′	8f	0.36(2)	0.625(9)	0.050(4)
Na3″	8f	0.16(2)	0.58(1)	0.040(5)
Ag4/Na4	8f	0.42(1)/0.09	0.927(3)/0.834(2)	0.0398(3)
Ag4′	8f	0.23(1)	0.819(9)	0.123(3)
Atoms		Distance/Å		
Na3–Na3′	×2	1.84(2)		
Na3–Na3″	×2	2.49(2)		
Na3′–Na3″		0.75(3)		
Ag4/Na4–Ag4′		0.50(1)		

[a] $U_{eq} = 1/3\left(\sum_{ij} U_{ij} a_i^* b_j^* a_i a_j\right)$.

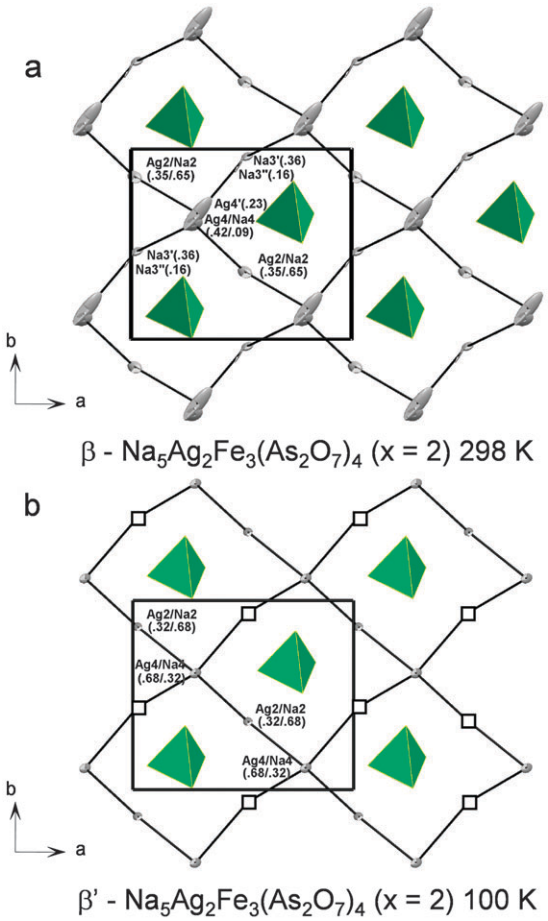

Fig. 5 Sodium/silver diffusion paths in the π2 plane of β at 298 K (a) and β′ at 100 K (b) of $Na_5Ag_2Fe_3(As_2O_7)_4$ (projection along [001]*). The occupancies are indicated in brackets.

Table 4 Wyckoff positions, site occupation factors, bond valence sums and equivalent isotropic displacement parameters for sodium/silver atoms in β′-$Ag_2Na_5Fe_3(As_2O_7)_4$ ($x = 2$) at 100 K. * refined close to unity

Atom	Wyck.	SOF	BVS	U_{eq}[a]/Å^2
Na1	8f	1*	1.128(5)	0.0042(5)
Ag2/Na2	8f	0.32(1)/0.68	0.951(4)/0.856(4)	0.0116(3)
Na3	4e	1*	1.180(6)	0.0185(9)
Ag4/Na4	8f	0.68(1)/0.32	0.925(4)/0.832(4)	0.0168(2)

[a] $U_{eq} = 1/3\left(\sum_{ij} U_{ij} a_i^* b_j^* a_i a_j\right)$.

is distributed in a strongly disordered manner in both kinds of sites except the "tunneling" M3′/M3″–M3. Here, the sodium appears as the most mobile species across this transition.

(2) $Na_2Ag_5Fe_3(P_2O_7)_4$ ($x = 5$) analysis of the α → β transition. At 298 K, the unit-cell of $Na_2Ag_5Fe_3(P_2O_7)_4$ ($x = 5$) is reminiscent of the standard β-form (Fig. 6a) *i.e.* characterized by disorder in the Na/Ag sites. The refinement started by using the coordinates of the known structure of β-$Na_7Fe_3(As_2O_7)_4$ for the $[Fe_3(P_2O_7)_4]$ framework. Fourier difference calculations allowed Ag1 and Ag2 silver sites to be located with partial occupancy and several sites too close to be simultaneously occupied: Ag3′, Ag3″, Ag3‴ and Ag4, Ag4′, Ag4″. At this stage of refinement, with SOF of all silver sites unconstrained, the obtained formulas were very close to $Ag_5Fe_3(P_2O_7)_4$. Additional Fourier difference syntheses allowed sodium Na3 atoms to be located, introduced with partial occupancies at the apex of split sites Ag3′, Ag3″ and Ag3‴. As the formula was deficient in sodium, mixed sites Ag/Na (Ag1/Na1 and Ag2/Na2) were introduced by restraining the sum of SOF. to be equal to 1, leading to the correct formula. The refinement of the anisotropic atomic displacement parameters for all atoms, a secondary extinction and unit weighting scheme led to reliability factors given in Table 2. Equivalent isotropic displacement parameters, BVS and selected interatomic distances for sodium/silver atoms for low and room temperature forms are reported in the Table 5. The important point here is that in this silver-rich composition, most of the remaining Na^+ ions of the structure remain within the M1 site, located in the B layer and not directly "connected" within the π diffusion planes.

The low temperature (100 K) form of α-$Na_2Ag_5Fe_3(P_2O_7)_4$ (Fig. 6b) is a tripled-cell superstructure of β (see above for relations) isostructural with α-$Na_7Fe_3(P_2O_7)_4$.[20] As in the β form, mixed sites M1 and M2 were considered as fully occupied. It is noteworthy that between two π-planes, on the

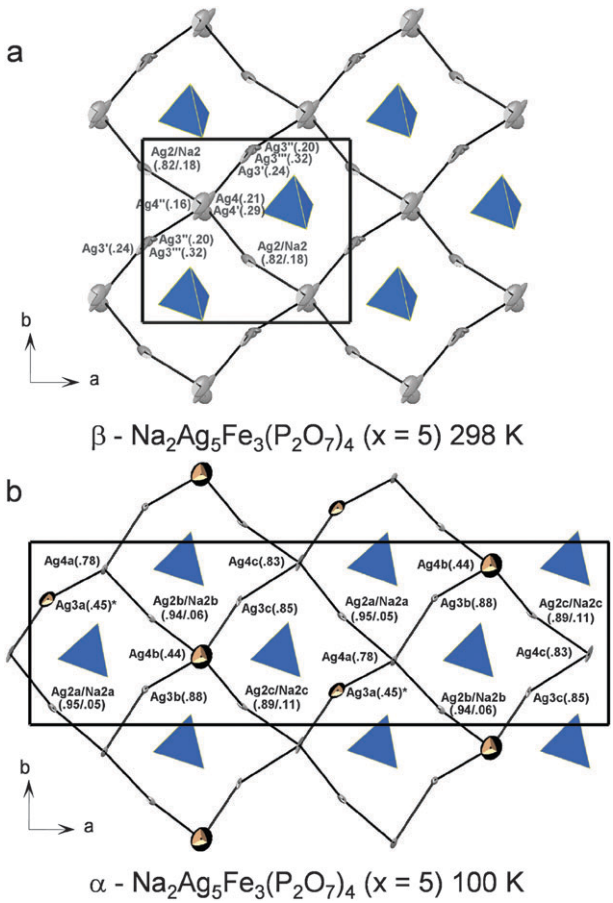

Fig. 6 Sodium/silver diffusion paths in the π2 plane of β at 298 K (a) and α at 100 K (b) of $Na_2Ag_5Fe_3(P_2O_7)_4$ (projection along [001]*). The occupancies are indicated in brackets. For the α form, the half-filled silver sites are shown in black. Ag3 sites with an asterisk are those at the apex of Na3 sites in (4e) position.

Table 5 Wyckoff positions, site occupation factors, bond valence sums, equivalent isotropic displacement parameters and selected interatomic distances for sodium/silver atoms in β-$Ag_5Na_2Fe_3(P_2O_7)_4$ (x = 5) at 298 K

Atom	Wyck.	SOF	BVS	U_{eq}[a]/Å^2
Ag1/Na1	8f	0.26(1)/0.74	1.264(2)/1.138(2)	0.0247(1)
Ag2/Na2	8f	0.82(1)/0.18	0.918(2)/0.826(1)	0.02877(7)
Na3	4e	0.16(1)	1.23(1)	0.050(5)
Ag3′	8f	0.240(8)	0.811(3)	0.0469(8)
Ag3″	8f	0.20(2)	0.847(7)	0.046(1)
Ag3‴	8f	0.32(2)	0.827(3)	0.0314(6)
Ag4	8f	0.21(1)	0.867(6)	0.085(1)
Ag4′	8f	0.290(7)	0.950(3)	0.0353(4)
Ag4″	8f	0.16(1)	0.824(7)	0.054(1)
Atoms		Distance/Å		
Na3–Ag3′	×2	2.291(3)		
Na3–Ag3″	×2	1.750(8)		
Na3–Ag3‴	×2	1.875(4)		
Ag3′–Ag3″		0.694(8)		
Ag3′–Ag3‴		0.462(4)		
Ag3″–Ag3‴		0.256(7)		
Ag4–Ag4′		0.339(7)		
Ag4–Ag4″		0.281(7)		
Ag4′–Ag4″		0.544(6)		

[a] $U_{eq} = 1/3\left(\sum_{ij} U_{ij} a_i^* b_j^* a_i a_j\right)$.

three possible midpath-like positions originating from Na3, only one at x = 1/2, y = 0.248(3), z = 1/4, is 55% occupied while the two remaining ones are empty. At their apex in the π-planes, we found almost fully occupied Ag3b and Ag3c sites while at the apex of Na3 (occ. = 0.55(1)) is located the half-filled Ag3a site (occ. = 0.45(1)). Finally, the sum of mixed Na/Ag sites were constrained according to the formula $Na_2Ag_5Fe_3(P_2O_7)_4$. A simple observation of the Na/Ag distribution shows an ordering with respect to homogenization of the electron density within π-planes. Thus, half-filled crossroads Ag4b are surrounded by squares of silver-rich M2b-M2c-Ag3b-Ag3c. Similarly half-filled midpath Ag3a are between two silver-rich crossroad-like Ag4a and Ag4c. It is also noticeable that the ellipsoids of Ag1b/Na1b, Ag3c and Ag4c are already strongly elongated at low temperature.

(B) Discussion and conclusion

The α → β′→ β transitions in silver/sodium ion conductors $Na_{7-x}Ag_xFe_3(X_2O_7)_4$ *i.e.* (x = 0 to 7; X = P, As) are clearly related to an order → disorder transition, accompanied by a reduction of the cell volume and an homogenization of the cationic density in π-planes. The present structural determinations provide very useful information on the mechanisms of 2D ionic diffusion and on the respective roles of each crystallographic site in the overall cation transport within the structure.

2D Ionic diffusion. The ionic transport properties of the limit compositions of the solid solutions $Na_{7-x}Ag_xFe_3(X_2O_7)_4$ *i.e.* (x = 0 to 7; X = P, As) were also investigated and show trends generally observed for Ag^+/Na^+ phosphate/arsenate ionic conductors. They are indicative of an Arrhenius-type behavior in the temperature range 25–300 °C with conductivities around 10^{-3}–10^{-2} S cm^{-1} at 300 °C. For compositions $x \neq 0$ and 7, no extra measurements were carried out, assuming a performance close to those already measured.[18,21]

It has already been stated for the limit compositions of the solid solutions $Na_{7-x}Ag_xFe_3(X_2O_7)_4$ (x = 0 and 7; X = P, As) that the most mobile Na^+/Ag^+ cations are located in A layer within parallel planes, so-called π.[18,21] The ionic diffusion paths were described as circumventing the XO_4 tetrahedra obstacles and following two possible directions $\sim\vec{a} + \vec{b}$ and $\vec{a} - \vec{b}$, then involving both midpath and crossroad sites. Thus, the Na1/Ag1 cations which are located within the B layer appear less involved in the overall ionic diffusion. Keeping in mind that the mixed compounds are prepared from Ag → Na exchanges, the four reported crystal structures clearly evidence that this site remains systematically filled by a majority of sodium cations. Even for x = 5, M1 contains ∼75% of sodium. By itself, this result corroborates the veracity of the proposed conductivity mechanism preferentially in the π-planes.

Also, the Na2/Ag2 mixed site within the A layer is the least influenced by the variation of temperature evidenced by the same configuration (one mixed site) and a SOF almost the same (.68/.32 at 100 K *vs.* .65/.35 at 298 K for the arsenate and .93/.07 at 100 K *vs.* .82/.18 at 298 K for the phosphate). This could illustrate that M2 positions are mobile and thus contribute less to the overall conductivity leading to a $\vec{a} + \vec{b}$ path favored over $\vec{a} - \vec{b}$ path.

The interplanar mobility is mediated by Na3 between two planes. This site is empty in silver-only phases[18] and, according to the present results, it is only partially Na-occupied in mixed compounds. At its apex within the planes ($z = \frac{1}{4}$), the M3′ satellites distribution is modified as a function of the composition and the temperature. In the arsenate, for x = 2, they are empty in the β′ form while Na3′ and Na3″ are progressively filled from the Na3 tank in the β form on heating. In the same manner, in the phosphate for x = 5, we already discussed the Ag3a–c → Ag3′–′–‴ strong redistribution accompanying the α → β transition. This pictures the crucial roles of these midpath like positions in the inter-planar diffusion.

Table 6 Wyckoff positions, site occupation factors, bond valence sums, equivalent isotropic displacement parameters and selected interatomic distances for sodium/silver atoms in α-$Ag_5Na_2Fe_3(P_2O_7)_4$ (x = 5) at 100 K

Atom	Wyck.	SOF	BVS	U_{eq}[a]/Å^2
Ag1a/Na1a	8f	0.18(1)/0.82	1.34(3)/1.20(3)	0.009(1)[b]
Ag1b/Na1b	8f	0.185(13)/0.815	1.35(3)/1.22(3)	0.012(2)
Ag1c/Na1c	8f	0.13(1)/0.87	1.34(3)/1.21(3)	0.003(1)[b]
Ag2a/Na2a	8f	0.95(1)/0.05	0.97(2)/0.88(2)	0.013(1)
Ag2b/Na2b	8f	0.94(1)/0.06	0.98(2)/0.88(2)	0.011(1)
Ag2c/Na2c	8f	0.89(1)/0.11	1.00(2)/0.90(2)	0.013(1)
Na3	4e	0.55(1)	1.19(3)	0.003(1)[b]
Ag3a	8f	0.45(1)	0.72(2)	0.077(4)
Ag3b	8f	0.88(1)	0.85(2)	0.024(1)
Ag3c	8f	0.85(1)	0.84(2)	0.028(1)
Ag4a	8f	0.78(1)	0.89(2)	0.011(1)
Ag4b	8f	0.44(1)	0.92(2)	0.094(6)
Ag4c	8f	0.83(1)	0.94(2)	0.024(1)
Atoms		Distance/Å		
Na3–Ag3a	×2	2.02(1)		

[a] $U_{eq} = 1/3\left(\sum_{ij} U_{ij} a_i^* b_j^* a_i a_j\right)$. [b] U_{iso}.

The analysis of thermal ellipsoids (U_{eq} & U_{aniso}) correlated to the BVS calculations (Table 3–6) gives a good picture of this deduced cationic mobility for each silver/sodium site from which several interesting trends may be highlighted confirming the previous statements:

The Na1/Ag1 and Na3 (4e) type sites systematically appear "overbonded" (BVS > 1) associated with the smallest thermal ellipsoid while all other splitted silver type atoms appear consistently "underbonded" (BVS < 1).

Na2/Ag2, Na3/Ag3 (excluded Na3 in (4e) site) and Ag4 type sites show ellipsoids lying in the in π-planes with vibrational elongations along the paths shown on Fig. 5 and Fig. 6. This "vibration" would represent the most probable silver/sodium diffusion paths. It is noticeable that BVS of Na2/Ag2 type sites appear systematically between BVS of Na1/Ag1/Na3(4*e*) and BVS of Ag3/Na3(not in 4e)/Ag4/Na4 type atoms validating our previous statement that the $\vec{a} + \vec{b}$ path seems to be favored over $\vec{a} - \vec{b}$ paths.

At 298 K, Ag3″ for the phosphate phase and Na3′ for the arsenate phase show an anisotropic ellipsoid oriented towards the parallel π-plane (along the [001] direction), suggesting a favorable π1 to π2 bridge.

Ag^+ *versus* Na^+ and influence of the size of framework. As showed by DSC data (Fig. 2), the transition temperature between the disordered β form and the ordered α form of $Na_{7-x}Ag_xFe_3(P_2O_7)_4$ decreases for $x = 0$ to 5, *i.e.* the diffusion of mobiles species needs to be less thermally activated with higher amounts of silver. This leads to the conclusion that silver cations have a better mobility than sodium cations. On going from the phosphate to the arsenate, the framework is expanded, which also has an impact on the order–disorder transition temperature: $Na_7Fe_3(P_2O_7)_4$ adopts the α form at 298 K; $Na_7Fe_3(As_2O_7)_4$ adopts the β form at 298 K.

For $x = 0$ and $x = 7$ compounds, at room temperature, X–O distances in XO_4 tetrahedra are in agreement with data from literature, varying from 1.494(2) to 1.629(3) Å (X = P)[18,20] and from 1.647(5) to 1.762(2) Å (X = As).[18,19] For $Na_2Ag_5Fe_3(P_2O_7)_4$ and $Na_5Ag_2Fe_3(As_2O_7)_4$, the X–O distances are very similar to those previously mentioned for a given X compound: from 1.497(2) to 1.628(2) ($x = 5$, X = P) and from 1.641(2) to 1.770(2) ($x = 2$, X = As). In silver compounds, we showed that the size of the $Fe_3(X_2O_7)^{7-}$ framework induced a more voluminous paths in the arsenates in good concordance with the biggest silver site splitting.[18] Interestingly, here, the site splitting is more important in the silver-rich ($x = 5$, X = P) than in the silver poor ($x = 2$, X = As) regardless of the nature of the X cations, confirming, despite the more voluminous path in the arsenate than in the phosphate compound, the predominant ability for mobility of the silver over the sodium atoms.

Acknowledgements

The "Fonds Européen de Développement Régional (FEDER)", "CNRS", "Région Nord Pas-de-Calais" and "Ministère de l'Education Nationale de l'Enseignement Supérieur et de la Recherche" are acknowledged for funding of single crystal X-ray diffractometers at the UCCS, Villeneuve d'Ascq, France.

References

1 J. Angenault, J. C. Couturier and M. Quarton, *Mater. Res. Bull.*, 1989, **24**(7), 789.
2 K. Koteswara Rao, G. Rambabu, M. Raghavender, G. Prasad, G. S. Kumar and M. Vithal, *Solid State Ionics*, 2005, **176**(37–38), 2701.
3 G. Rambabu, N. Anantharamulu, K. Koteswara, G. Prasad and M. Vithal, *Mater. Res. Bull.*, 2008, **43**, 1509.
4 A. Daidouh, C. Durioa, C. Pico, M. L. Veigaa, N. Chouaibi and A. Ouassini, *Solid State Sci.*, 2002, **4**, 541.
5 A. Daidouh, M. L. Veiga and C. Pico, *J. Solid State Chem.*, 1997, **130**, 28.
6 H. Fukuoka, H. Matsunaga and S. Yamanaka, *Mater. Res. Bull.*, 2003, **38**, 991.
7 M. Meunier, R. Izquierdo, L. Hasnaoui, E. Quenneville, D. Ivanov, F. Girard, F. Morin, A. Yelon and M. Paleologou, *Appl. Surf. Sci.*, 1998, **127–129**, 466.
8 S. Yao, Y. Shimizu, N. Miura and N. Yamazoe, *Chem. Lett.*, 1990, 2033.
9 R. Collongues, A. Khan and D. Michel, *Annu. Rev. Mater. Sci.*, 1979, **9**, 123.
10 J. Alamo and R. Roy, *J. Mater. Sci.*, 1986, **21**, 444.
11 R. Roy, E. R. Vance and J. Alamo, *Mater. Res. Bull.*, 1982, **17**, 585.
12 A. Serghini, A. Kacimi, M. Ziyad and R. Brochu, *J. Chem. Phys.*, 1988, **85**, 499.
13 N. Hirose and J. Kuwano, *J. Mater. Chem.*, 1994, **4**, 9.
14 A. Nadiri and C. Delmas, *C. R. Acad. Sci. Paris*, 1987, **304**, 9.
15 C. Delmas, F. Cherkaoui, A. Nadiri and P. Hagenmuller, *Mater. Res. Bull.*, 1987, **22**, 631.
16 C. Delmas, A. Nadiri and J. L. Soubeyroux, *Solid State Ionics*, 1988, **28–30**, 419.
17 J. Gopalakrishnan and K. Kasturi Rangan, *Chem. Mater.*, 1992, **4**, 745.
18 E. Quarez, O. Mentré, Y. Oumellal and C. Masquelier, *New J. Chem.*, 2009, **33**, 998.
19 C. Masquelier, F. D'Yvoire and N. Rodier, *Acta Crystallogr., Sect. C: Cryst. Struct. Commun.*, 1990, **46**, 1584.
20 C. Masquelier, F. D'Yvoire and N. Rodier, *J. Solid State Chem.*, 1991, **95**, 156.
21 C. Masquelier, F. D'Yvoire, E. Bretey, P. Berthet and C. Peytour-Chansac, *Solid State Ionics*, 1994, **67**, 183.
22 J. Rodriguez-Carjaval, *Fullprof suite*, LLB (CEA-CNRS), France, 2000.
23 *SMART*, Siemens Analytical X-ray Systems, Inc., Madison, WI 53719.
24 SAINT + Version 6.02: Area-Detector Integration Software, Siemens Industrial Automation, Inc.: Madison, WI 1998.
25 G. M. Sheldrick, *SHELXTL NT*, version 5.1, Bruker Analytical X-ray Systems, 1998.
26 *SADABS: Area-Detector Absorption Correction*, Siemens Industrial Automation Inc., Madison, WI, 1996.
27 V. Petricek, M. Dusek and L. Palatinus,*The Crystallographic Computing System*, Institute of Physics, Praha, Czech Republic, 2006.
28 I. D. Brown and D. Altermatt, *Acta Crystallogr., Sect. B: Struct. Sci.*, 1985, **41**, 244.